α-Cu2Se thermoelectric thin films prepared by copper sputtering into selenium precursor layers

P. Fan, X.-L. Huang, T.-B. Chen, F. Li, Y.-X. Chen, B. Jabar, S. Chen, H.-L. Ma, G.-X. Liang, J.-T. Luo, et al.

α-Cu_2Se thermoelectric thin films prepared by copper sputtering into selenium precursor layers

Ping Fan [a], Xiao-lan Huang [a], Tian-bao Chen [a, b], Fu Li [a], Yue-xing Chen [a], Bushra Jabar [a], Shuo Chen [a], Hong-li Ma [b], Guang-xing Liang [a], Jing-ting Luo [a], Xiang-hua Zhang [b], Zhuang-hao Zheng [a, *]

a Shenzhen Key Laboratory of Advanced Thin Films and Applications, Key Laboratory of Optoelectronic Devices and Systems of Ministry of Education and Guangdong Province, College of Physics and Optoelectronic Engineering, Shenzhen University, Shenzhen 518060, P. R. China;

b Univ Rennes, CNRS, ISCR (Institut des Sciences Chimiques de Rennes) UMR6226, Rennes F-35000, France.

[*] Corresponding author. E-mail: zhengzh@szu.edu.cn

Abstract Copper selenide (Cu_2Se) is a promising thermoelectric material and α-phase Cu_2Se provides relatively safe thermoelectric modules for thin film thermoelectric device in contrast to some toxic materials currently on the market. In this work, nanocrystalline Cu_2Se thin film with uniform element distribution was fabricated at room temperature through an effective combination reaction method by implanting sputtered Cu^+ ions into Se precursor. Then, self-assembled growth of Cu_2Se thin films with desired α-phase and well crystallinity was successfully achieved with optimization of annealing temperature. Interestingly, the growth orientation has obviously affected by the annealing temperature, which significantly affects the thermoelectric properties. Consequently, the Seebeck coefficients increase with the increase in the orientation factor of the (0*l*0) preferred orientation, which enhances power factor. The high maximum power factor of 9.23 $\mu Wcm^{-1}K^{-2}$ is achieved for α-Cu_2Se thin film with (0*l*0) preferred orientation, demonstrating that the method used in this work has great potential in developing low-cost and high-performance thermoelectric thin films from relatively earth-abundant elements.

Keywords thermoelectric, copper implant, α-Cu_2Se thin films, crystal structure

1. Introduction

Thermoelectric (TE) materials can directly convert heat into electric energy, and vice versa; this capability is important to develop clean, secure, sustainable, and convenient energy sources.[1] The performance of TE materials is determined or defined by a dimensionless figure of merit $ZT = (S^2\sigma/\kappa)$T, where S, σ, κ, and T are the Seebeck coefficient, electrical conductivity, thermal conductivity, and absolute temperature, respectively. The parameter $S^2\sigma$, which is called the power factor (PF), is also usually used to estimate their TE performance.[2] With the rapid rise of portable and wearable microelectronics in recent years, TE thin film materials have received great attention as a promising miniature, convenient, and self-powered electronic component in a TE device.[3] Thus far, considerable efforts have been devoted to develop the potential applicable TE thin film of Bi_2Te_3 at/near room temperature. Various methods have been applied to prepare TE thin films,[4-8] and the most studied ones are low-temperature TE materials determined by the potential practical applications of thin film devices.[9-12] However, Bi_2Te_3 remains a significant challenge for large-scale commercialization despite of its considerable progresses to date [13-15] due to the presence of less earth-abundant, toxic, and costly elements. Thus, developing low-cost and nontoxic TE thin films with acceptable performance to substitute Bi_2Te_3-based materials is highly desired.

In recent decades, new strategies have been used to orient the discovery of new eco-friendly bulk TE materials, [16-20] especially chalcogenides, such as Sn-based, [21] Cu-based, [22] and Ag-based [23] chalcogenides. These materials have high ZT values in a wide range of operating temperature by doping, and this condition introduces atomic scale lattice defects and nano-scale precipitates. In the abovementioned context, copper selenide (Cu_2Se) has attracted considerable attention due to its excellent TE performance with simple crystal structure and low-cost Cu and Se. It offers exciting opportunities in commercialization, the theoretical prediction of relatively large ZT values at/near room temperature, and experimental demonstration of high ZT values in bulk Cu_2Se since Liu et al. reported an

intrinsically high *ZT* value in bulk Cu_2Se [24]. To date, many theoretical and experimental studies have established that the *ZT*s of Cu_2Se TE materials can be higher than 2 at a high temperature ranging from 800 K to 1000 K due to the "liquid-like" behavior of the anti-fluorite-structured β-phase.[25] However, bulk Cu_2Se with monoclinic structured α-phase also exhibits good TE performance at near room temperature.[26] For example, Day et al. reported that the theoretical prediction of the maximum *ZT* of α-Cu_2Se is approximately 1.16 at 305 K, which can be compared with that of the commercial traditional TE materials.[27] Chen et al. synthesized the Bi-doped α-Cu_2Se by using spark plasma sintering method and achieved the high *ZT* value over 0.4 at 373 K.[28] To this end, α-Cu_2Se is a good candidate that is expected to achieve high performance near room temperature and thus serves as a potential alternative for the traditional Bi_2Te_3-based TE.

High TE performance realized in bulk Cu_2Se thin films has also received much attention. Various fabrication techniques have been used to enhance *ZT* or *PF* of Cu_2Se-based thin films.[29-32] For instance, Lin et al. prepared Cu_2Se thin film by using solution method, which resulted in maximum *PF* of 6.2 and 4.6 $\mu Wcm^{-1}K^{-2}$ on rigid Al_2O_3 substrate and flexible polyimide substrate, respectively.[33] Scimeca et al. optimized the carrier concentration of Cu_2Se thin films through a soaking process in Cu^+ ion solution, which significantly improved their TE properties.[34] However, the reported Cu_2Se thin films to date usually exhibit low TE performance mainly due to structural imperfections, including voids and component defects in the films. High-temperature post treatment is also always used to further improve and stabilize the TE performance of the thin film. However, this method often weakens the bonding strength between thin film and substrate (especially between thin film and the organic flexible substrate). Thus, reasonably designing and fabricating Cu_2Se thin film with excellent TE performance while avoiding high-temperature processing are difficult.

Among the abovementioned deposition techniques, magnetron sputtering is a well-established approach that has been extensively utilized to prepare high-performance TE thin

films. [35-39] It has the advantages of precise composition control, excellent uniformity, and simple experimental setup. However, only a few attentions have been paid on the investigation of magnetron-sputtered Cu_2Se thin films to date. Thus, further research is needed to improve the TE performance of Cu_2Se thin film. However, effective composition control and low-temperature synthesis process of Cu_2Se are challenging because high-temperature treatment process can cause the precipitation and re-evaporation of Se, which lead to Se deficiency defects. In this work, a two-step simple and novel combination reaction route was utilized to implant sputtered Cu^+ ions into Se precursor. Furthermore, the self-assembled growth of α-Cu_2Se thin films with desired crystallinity was successfully realized by adjusting the annealing process. Moreover, the precursor Se layer was prepared using thermal evaporation method instead of using sputtering method, which is more efficient and controllable than selenium deposition by employing sputtering method. Importantly, the magnetron-sputtered Cu^+ ions have high energy and can be uniformly implanted into the Se layer. They can combine with Se with the crystallized structure, which can reduce the reaction temperature at the subsequent annealing process. Consequently, the Seebeck coefficients are significantly improved by adjusting the annealing temperature to control the preferred orientation, which leads to a high *PF* value of 9.23 $\mu Wcm^{-1}K^{-2}$ of α-Cu_2Se thin film.

2. Experimental Section

A schematic of the whole process of the Cu_2Se thin film fabrication is illustrated in Figure 1. First, Se precursor layer was fabricated using thermal evaporation deposition method. High-purity Se powder (>99.99%) with the weight of 0.1 g was evenly placed at a tungsten container in the vacuum thermal evaporation system. Before deposition, glass substrate was ultrasonically sequentially and then cleaned with industrial detergent, deionized water, and alcohol sequentially for 30 min. The distance between the substrate and the source was approximately 30 cm, and the background pressure was evacuated below 5.0×10^{-4} Pa. The heating current of the evaporation source was 60 A with the heating rate of 10 A/min. The

average deposition rate of Se was around 0.8 Å/s, and the total thickness of Se precursor layer was 80 nm. Subsequently, Cu ions were implanted into the Se precursor layer by using magnetron sputtering deposition. The Cu target (99.99%) was fixed in a magnetron sputtering facility, and the prepared Se thin film sample and a blank glass substrate were set at the substrate holder. The sputtering angle was 45°, and the target–substrate distance was 10 cm. The vacuum chamber was first pumped down to 8.0×10^{-4} Pa. Then, Ar with high purity (>99.99%) was introduced into the sputtering chamber at a flow rate of 35 sccm. The working pressure and sputtering power were kept at 0.6 Pa and 30 W, respectively. The sputtering duration was fixed to be 10 min for all samples to deposit a Cu layer with 100 nm (measured from the blank glass substrate). Finally, the annealing process was utilized with a slow heating rate (nearly 2 °C/min) in a glove box filled with nitrogen. The annealing temperature was varied from 100 °C to 240 °C with the interval temperature of 20 °C for 60 min.

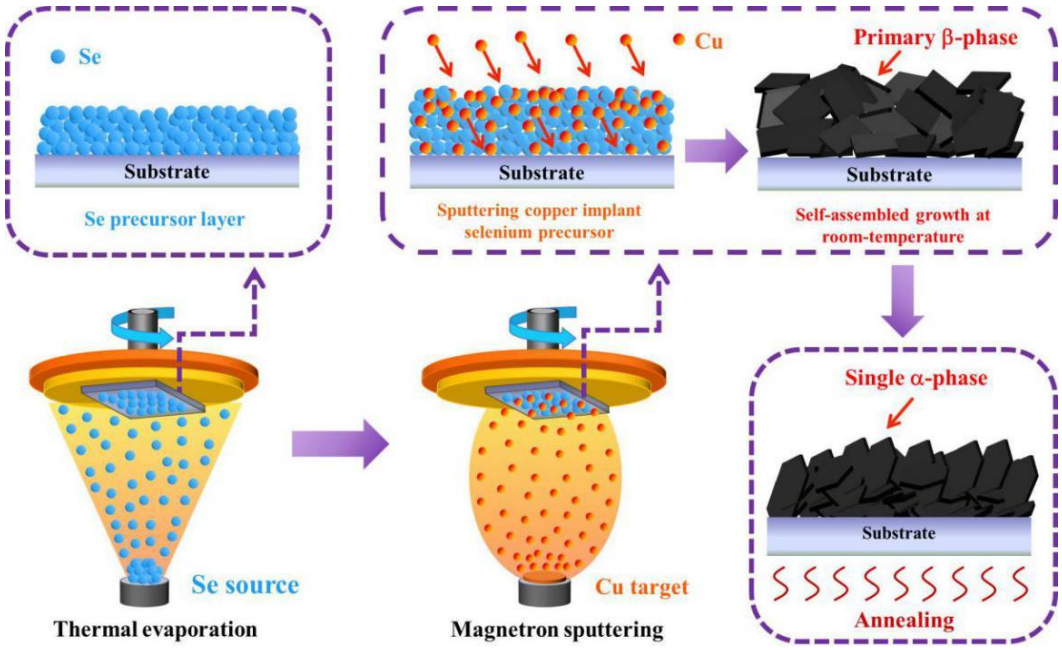

Figure 1 Schematic of the fabrication of α-Cu_2Se thin films.

Surface and cross-sectional microstructures of the Cu_2Se thin film were characterized using a scanning electron microscope (SEM, Supra 55) with an electron beam accelerated of 5 kV. Crystal structure of the thin films was investigated by X-ray diffraction (XRD, Ultima-iv)

with the 2θ angle range from 10 ° to 60 ° by using CuK_α radiation (under operation conditions of 40 kV and 40 mA). Chemical compositions were analyzed using an energy dispersive X-ray spectroscope (EDS, Bruker Quantax 200) equipped with the SEM. The depth composition distribution throughout the thickness of the thin film was investigated by Auger scanning system (AES, PHI-700, Ulvac-Phi). The incident angle of scanning Argun was 30° with the sputter rate of 4 nm/min for standard SiO_2 sample. The chemical valence was determined by conducting X-ray photoelectron spectroscopy (XPS, Escalab 250Xi) with a monochromatic Al K_α X-ray source of 1486.6 eV. Samples were subjected to plasma etching for 30 seconds before the measurement in order to remove the oxide layer on the thin film surface. Transmission electron microscopy (TEM, JEM-3200FS) was used to investigate the microstructure of the thin films. The thickness of the thin film was measured using a profilometer (Dektak XT, Bruker). The Seebeck coefficient and electrical conductivity were measured by the Seebeck coefficient/electrical resistance measuring system (ZEM-3M10, Advance Riko). The uncertainties of the measurements were taken as 5 %, and uncertainties of $S^2\sigma$ were estimated to be around 10%. The carrier concentration and mobility were measured by Van der Pauw Hall measurement (HL5500PC, Nanometrics). The electrostatic potential calculations of Cu_2Se bilayer were implemented by the Vienna ab initio simulation package (VASP) [40-41]. The exchange–correlation functional was dealt with the generalized gradient approximation at Perdew–Burke–Ernzerhof (PBE) level. The first Brillouin zone was integrated by using the Monkhorst–Pack scheme of k-point sampling, and the cutoff energy for the expansion of plane-wave function was set at 450 eV. A vacuum of 16 Å perpendicular to the 2D plane was used to demonstrate a finite layer of LHS. K-point sampling of 15×15×1 was set for geometry optimization and static total energy calculations. The convergence criteria were restricted to less than 10^{-5} eV for energy and 0.01 eV/Å in force.

3. Results and Discussion

Figure 2a displays the energy dispersive X-ray spectroscope mapping images of the as-

deposited thin film and indicates that the Cu and Se have uniform distribution in the in-plane direction. The Auger scanning system depth analysis (Figure S1, Supporting information) shows that the atomic ratio of Cu to Se is close to 2:1 with slight Cu deficiency. Moreover, Cu and Se are homogeneous throughout the thickness of the thin film layer. These results reveal that the sputtered Cu ions are successfully implanted uniformly into the Se precursor layer.

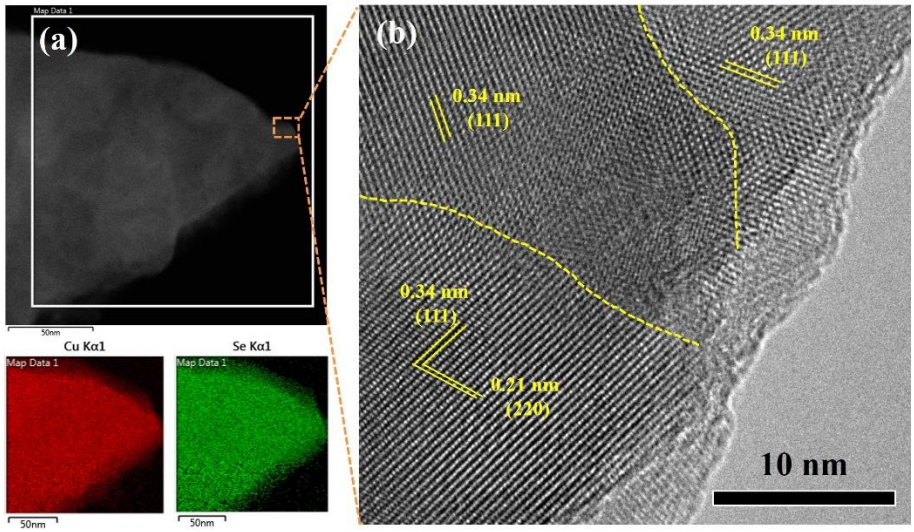

Figure 2 TEM characterization and EDS elemental mappings of the as-deposited Cu_2Se thin film (a). Lattice fringes of the as-deposited thin film in (a) performed by HRTEM are shown in (b).

XRD, SEM, and TEM were performed to further investigate the microstructure of the as-deposited sample. Unlike the amorphous thin films prepared at room temperature in the most cases, [42-44] XRD result (Figure S2, supporting information) exhibits that the as-deposited sample is crystalline. Most diffraction peaks are well indexed to the β-Cu_2Se phase (PDF#65-7737), and some peaks belong to the α-phase Cu_2Se secondary phase. The insert SEM image in Figure S2 clearly shows a relatively flat surface containing uniformly sized nano-grains with tens of nanometers. Figure 2b shows the high-resolution TEM image and represents that the as-deposited sample is composed of multiple crystalline nanoparticles that stack compactly with each other. The measured lattice spacings are 0.34 nm and 0.21 nm, which correspond to the (111) and (211) planes of the β-phase Cu_2Se, respectively. This finding is

consistent with XRD result. Apparently, a self-assembled nanocrystalline Cu_2Se thin film is successfully fabricated at room temperature by this novel combined reaction method. Unexpectedly, the as-deposited sample shows a mixture phase, and β-phase is the dominant phase. This result is consistent with the phase diagram presented by Kang et al. that two-phase mixture structure could be obtained at room temperature in a non-stoichiometry Cu_2Se system.[45] However, although β-phase-structured Cu_2Se has ultralow thermal conductivity and good electrical transport properties at high temperature due to the "phonon liquid electron-crystal" behavior, high carrier concentration always results in low TE performance near room temperature. The room-temperature electrical transport measurement in table S1 (Supporting information) confirms this deduction that the as-deposited sample has low Seebeck coefficient due to the considerable high carrier concentration. For low-temperature TE applications, the α-phase monoclinic Cu_2Se with minimal structural defect is preferred because it has a lower carrier concentration than the β-phase. Annealing process has been proven as a crucial factor for perfecting microstructure and TE performance of thin films in our previous reports.[46] Therefore, the annealing process was employed, and the effect of annealing temperature on the microstructure and TE performance of Cu_2Se thin film was investigated.

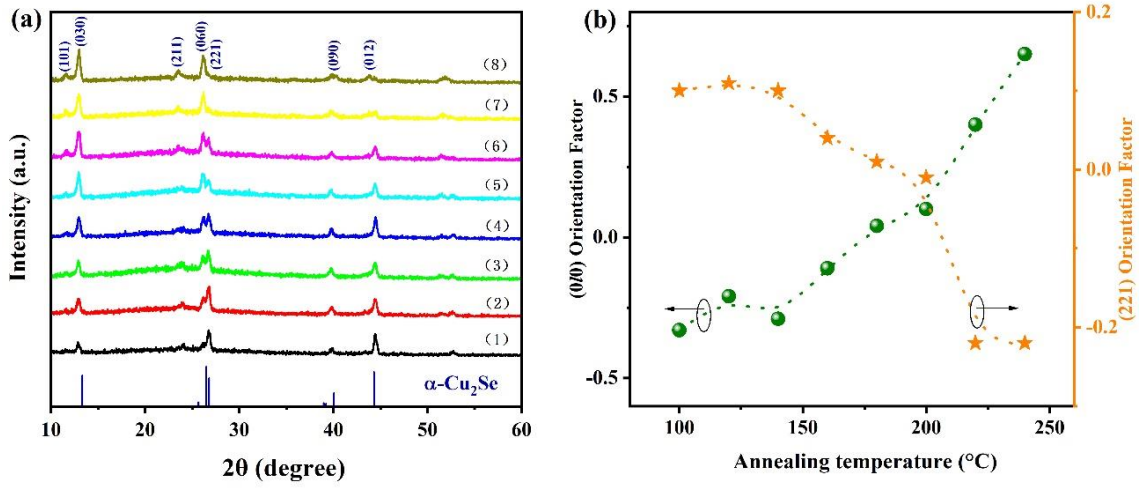

Figure 3 (a) XRD data of Cu_2Se thin films prepared at different annealing temperatures

measured at room temperature, (1) 100 °C, (2) 120 °C, (3) 140 °C, (4) 160 °C, (5) 180 °C, (6) 200 °C, (7) 220 °C, and (8) 240 °C. (b) Orientation factor of (0l0) and (221) diffraction peaks. The thickness of the thin films is shown in table S2 (Supporting information) and displays that the thickness did not change obviously after annealing. Figure 3a shows the XRD patterns of the Cu_2Se samples fabricated at various annealing temperature. As observed, all the thin films have primary α-phase after annealing and the intensity of main diffraction peaks increases with the increase of annealing temperature, indicating the well-crystallinity of the thin films. This finding suggests that the stable Cu_2Se thin films of α-phase crystal are successfully prepared. Notably, the peak intensity of the (211) plane is highest when the annealing temperature is < 160 °C, and the peaks of the (0*l*0) planes become stronger as temperature further increases. This phenomenon indicates the change in the preferred orientation growth characteristics. Orientation factor (*F*), which is an indicator of preferred crystal orientation, was applied to further quantitatively investigate the orientation preference of the samples by using the following equation:[47]

$$F = \frac{P - P_0}{1 - P_0} \tag{1}$$

$$P = \frac{I(0l0)}{\sum I(hkl)} \tag{2}$$

$$P_0 = \frac{I_0(0l0)}{\sum I_0(hkl)} \tag{3}$$

where I(0*l*0) is the sum of the diffraction intensity of (0*l*0) planes, ΣI(*hkl*) is the total intensity of all (*hkl*) diffraction peaks and P is the ratio of the intensity of (0*l*0) plane in the measured data. In the same way, the $I_0(0l0)$, $I_0(hkl)$, and P_0 represent the corresponding ones from the standard pattern. As shown in Figure 3b, the $F_{(0l0)}$ orientation factor increases from −0.33 to 0.65 with the increase in annealing temperature, while the $F_{(211)}$ orientation factor decreases from 0.10 to −0.22 with the increase in annealing temperature. Therefore, the thin films have

(0*l*0) preferred orientation at T ≥ 180 °C. According to the previous reported data[48-51], the preferred orientation significantly affects the charge carrier transport, which therefore affects the TE properties of the thin film.

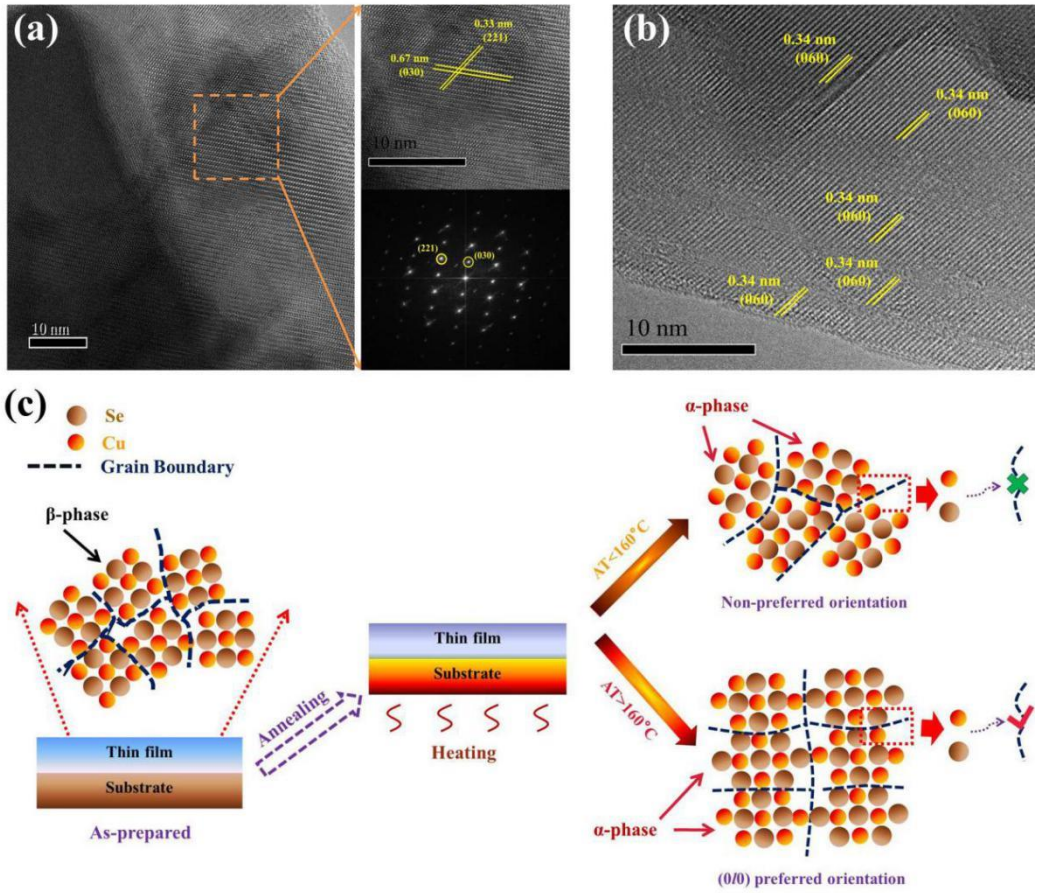

Figure 4 HRTEM images of the α-Cu_2Se thin films annealed at (a) 160 °C and (b) 240 °C. (c) Schematic of the preferred growth orientation of the α-Cu_2Se thin films in different annealing temperatures.

The surface morphology of the thin films annealed at different temperatures measured by SEM is shown in Figure S3 (Supporting information). Similar to the as-deposited sample, a smooth surface is observed from the sample annealed at 100 °C. Some flake-like particles are observed on the surface of the thin film, and the particle size and amount increase with the increase in annealing temperature. Eventually, a dense surface with compact flake-like grains is achieved as the annealing temperature reaches 240 °C. The cross-sectional images (Figure S4, supporting information) show that the samples (annealed at <160 °C) have grains mostly

grown in parallel to the surface, where some of grains are perpendicularly embedded. For the samples annealed at >160 °C, the grains have obvious columnar growth characterization. As confirmed from the XRD result, such difference is anticipated due to the change in the preferred growth orientation of the thin films at various annealing temperatures. The high-resolution TEM analysis of the sample annealed at T=160 °C and T=240 °C was performed to further investigate the change in the microstructure. As shown in Figure 4a, no impurity phase and amorphous region can be observed from the sample annealed at 160 °C. The measured lattice spacings are 0.67 and 0.33 nm, which correspond to the (030) and (221) planes of the α-phase Cu_2Se, respectively. Therefore, the sample has single α-Cu_2Se crystal structure with few structural defects. This finding is consistent with the XRD result. However, no obvious preferential growth orientation of the grains is observed from the thin film annealed at 160 °C. Figure 4b shows that the grains compactly stack with each other with the same (0*l*0) direction as the sample annealed at T=240 °C, which demonstrates that the sample has (0*l*0) preferred growth orientation. The schematic of the change in the preferred orientation at different annealing temperatures is shown in Figure 4c for further revealing the mechanism of growing process of the α-Cu_2Se. As we mentioned above, the grains with β-phase crystal structure are stack randomly with each other for the as-prepared thin film. At low-temperature annealing (T<160 °C), the atoms are rearranged and recrystallized into a more stable α-phase structure. However, most of the Cu and Se atoms cannot migrate through previously formed grain boundaries due to certain reasonable limits of diffusion energy at low temperature. Thus, the grains remain randomly stacked, which results in non-preferred growth. With the increase in annealing temperature, the atoms can migrate through the grain boundary and grow epitaxially to a certain preferential orientation. Specifically, the annealing method used in this work is to heat the bottom of the substrate. Thus, the atoms will preferably migrate through the temperature field (perpendicular to the substrate), which causes the high preferred orientation of (0*l*0).

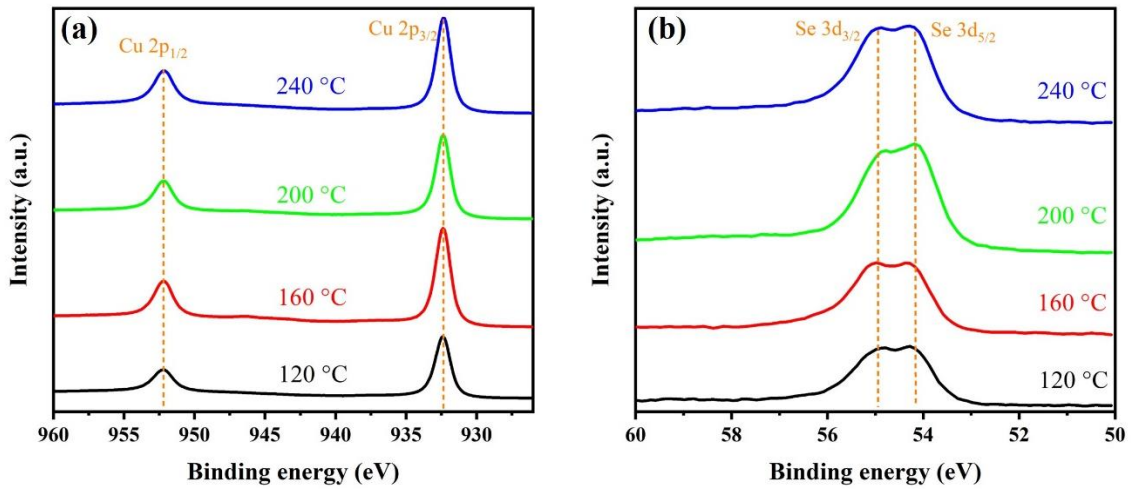

Figure 5 XPS spectra of samples annealed at 120 °C, 160 °C, 200 °C and 240 °C: (a) Cu and (b) Se

XPS measurement was conducted on representative thin films annealed at 120 °C, 160 °C, 200 °C and 240 °C to examine the binding states of α-phase Cu_2Se thin films. The core level spectrum in Figure 5a reveals that two strong peaks are obtained at ~932.4 eV of Cu $2p_{3/2}$ and ~952.2 eV of Cu $2p_{1/2}$ for all the spectrums, which are well matched with the spin–orbit phenomena of Cu (I) [52]. Interestingly, no impurity peak can be observed from the spectrums, demonstrating that no Cu oxidized state. By combining the EDS result that the overall oxygen content is rather low (Figure S5, supporting information), it can confirm that the thin films have well environmental stability. As illustrated in Figure 5b, a broad peak ranging from 52–56 eV is observed and can be identified into two symmetric peaks to be assigned to Se $3d_{5/2}$ and Se $3d_{3/2}$ located at ~54.2 and ~54.9 eV, which is the characteristic shape of Se (−II) in a consistent bonding environment.[53] Thus, these analyses indicate that the chemical states of the elements of the thin films are single Cu^{1+} and Se^{2-}. Additionally, few changes can be observed from the peak position in both Cu and Se, indicating that both Cu and Se have stable valance state in the annealed samples.

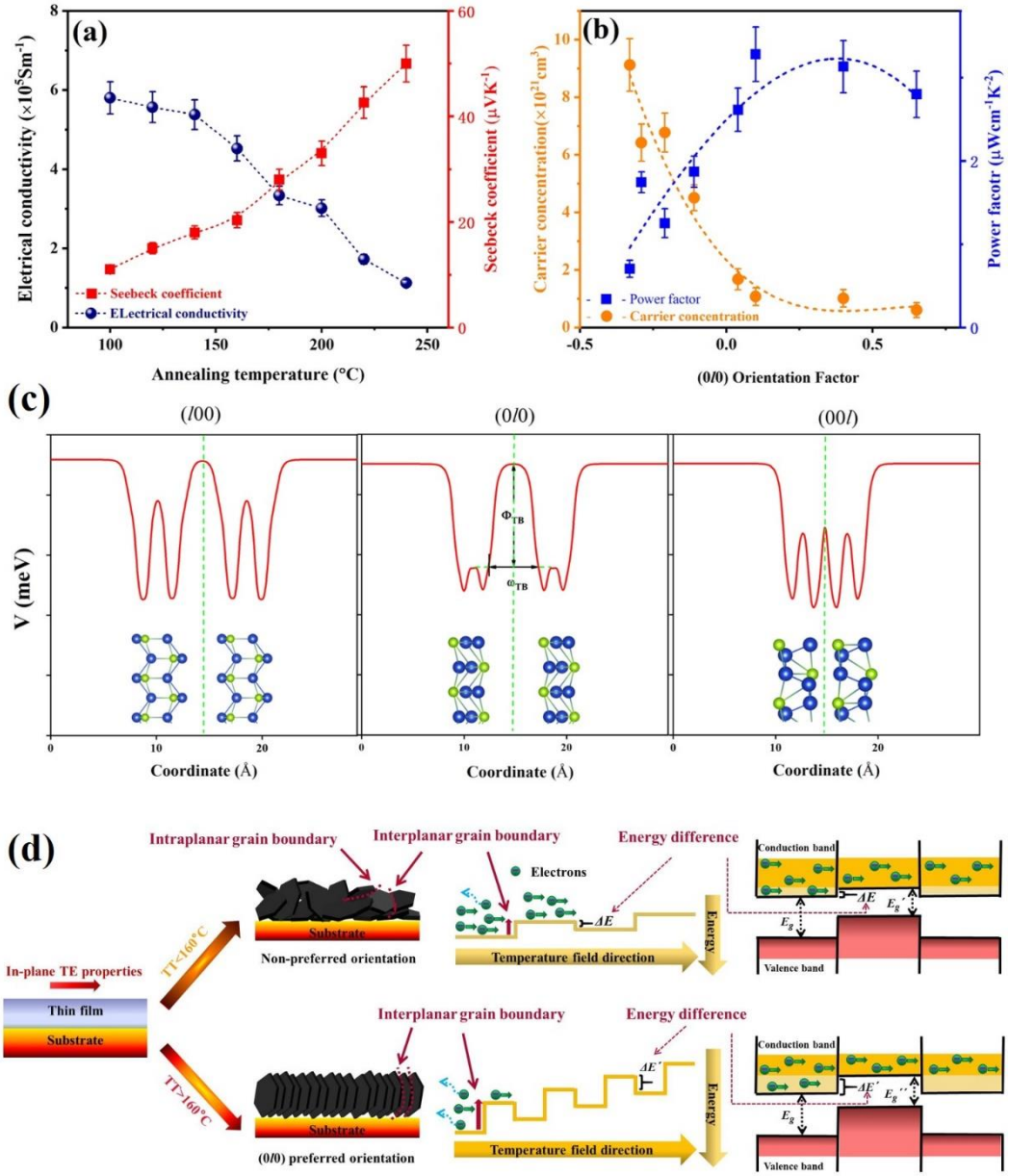

Figure 6 (a) Room-temperature Seebeck coefficient and electrical conductivity as a function of annealing temperature. (b) Carrier concentration and power factor of the thin films as a function of *F*s of (0*l*0) diffraction peak. (c) Averaged electrostatic potential between different interface of Cu_2Se grains in the direction of (*l*00), (0*l*0) and (00*l*). (d) Schematic of the influence of the preferred orientation on the in-plane electrical transport of the thin films.

The in-plane room-temperature Seebeck coefficient *S* and electrical conductivity σ of the thin films are shown in Figure 6a. The positive *S* indicates that all the thin films are p-type semiconductors. The *S* value increases with the increase in annealing temperature, while σ

shows the opposite trend. The EDS analysis (Figure S6, supporting information) reveals that, although the Se content decreases with the increase in annealing temperature, the change in the Se content can be ignored within the detection limit of EDS. Thus, the change in S and σ are mainly attributed to the change in the (0l0) preferred growth orientation. Indeed, σ and S can be written by the following formulas.[54]

$$\sigma = n\mathrm{eu} \quad (4)$$

$$S = \frac{8\pi^2 k_B^2 T m^*}{3eh^2}\left(\frac{\pi}{3n}\right)^{2/3} \quad (5)$$

where n is the carrier concentration, u is the hall mobility, k_B is the Boltzmann's constant, m* is the effective mass of the carrier, and h is the Planck constant. The carrier concentration was measured by Van der Pauw Hall measurement. Figure 6b shows the effect of $F_{(0l0)}$ on the carrier concentration of the samples. As observed, the carrier concentration decreases with the increase in $F_{(0l0)}$, and this condition significantly decreases the electrical conductivity. Conversely, lower carrier concentration is beneficial to achieve higher S value. To understand more fundamental cause of carrier transfer along different directions, the 2D plane averaged electrostatic potential of Cu_2Se bilayer along the vacuum direction is shown in Figure 6c. Here, the three most representative of Cu_2Se bilayer are selected with the interface directions perpendicular to (l00), (0l0) and (00l), respectively. It displays that three direction systems possess different height (Φ_{TB}) and width (ω_{TB}) of potential barrier, suggesting different carrier tunneling performances between them. More detailedly, as low-energy carriers can be filtered out by the grains interface, the higher Φ_{TB} and ω_{TB} of potential barrier along (0l0) direction indicating a lower carrier tunneling probability than two others. With the increase of the annealing temperature, the orientation factor $F_{(0l0)}$ increases, means that more grains interface along the (0l0) direction occupies which will scatter more carries, resulting in the decrease of carrier concentration. Thus, the effect of the change in growth orientation on the TE performance of in-plane thin films are schematically illustrated in Figure 6d. Under low-

temperature annealing, no obvious preferred orientation is observed, which indicates the disorder grain boundaries with formed interplanar and intraplanar. As the thin film grows preferentially within the (0*l*0) orientation at high annealing temperature, the interplanar grain boundaries become dominant along the perpendicular in-plane direction. Such a structural change results in the enhanced electron scattering, which is represented by lower carrier concentration and correspondingly relatively lower electrical conductivity. By contrast, the relatively increased interplanar grain boundaries might introduce more interface barrier, which acts as additional energy filtering effect; this condition ultimately increases high-energy electrons and correspondingly achieves higher *S*. [54] The calculated power factor *PF* is also shown in Figure 6b. This factor shows an increasing trend with the increase in $F_{(0l0)}$. The optimized *PF* with the value of 3.27 $\mu Wcm^{-1}K^{-2}$ is obtained at $F_{(0l0)}$ of 2.3, and further increase in $F_{(0l0)}$ leads to the decrease in *PF*.

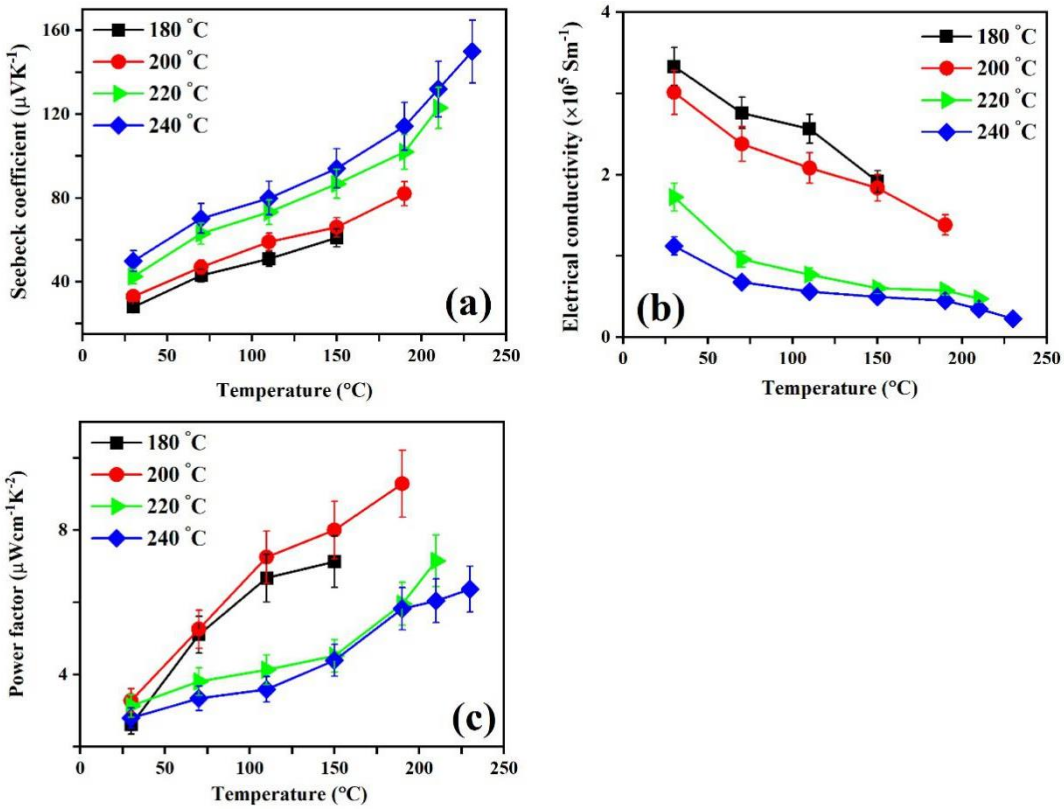

Figure 7 Temperature dependence of Seebeck coefficient (a), Electrical conductivity (b) and Power factor (c) of thin films with high (0*l*0) preferred orientation.

The temperature-dependent in-plane *S* and σ of the samples with high $F_{(0/0)}$ value were measured up to the corresponding annealing temperature to avoid any additional undesired structural change during the measurement, as shown in Figures 7a and 7b. As test temperature increases, the *S* value of all the thin films increases while the σ value decreases. The sample annealed at 240 °C has highest Seebeck coefficient among the thin films in the whole test temperature range and achieves a high value of 150 μVK^{-1} when the test temperature reaches 230 °C. Conversely, the samples annealed at lower temperature have higher σ values. The calculated *PF* values as a function of temperature are shown in Figure 7c. The value displays a similar increasing trend to that of Seebeck coefficient. The samples annealed at 180 °C and 200 °C have higher *PF* than that of the thin films annealed at higher temperature due to the decrease in electrical conductivity. The maximum *PF* value among all the thin films is found to be 9.23 $\mu Wcm^{-1}K^{-2}$ from the sample annealed at 200 °C. Additionally, the repeatability measurement of the sample annealed at 200 °C is shown in Figure S7 (Supporting information), and the results displays that the sample has significantly high repeatability and stability. Table S3 shows that the obtained high *PF* for the present thin film is comparable to the corresponding parameters reported in typical Cu_2Se thin film systems [53-60]. This consistency clearly demonstrates the efficiency of this innovative technique for preparing high-performance and low-cost α-phase Cu_2Se TE thin film.

4. Conclusion

Well-crystallized α-Cu_2Se TE thin films have been synthesized by sputtering copper implant selenium precursor method. The preferred growth orientation of the thin films can be efficiently adjusted by the annealing temperature, which significantly affects the carrier concentration. This condition ultimately decreases the electrical conductivity and increases the Seebeck coefficient. The maximum power factor of 9.23 $\mu Wcm^{-1}K^{-2}$ is achieved after annealing temperature optimization, which can be is one of the best values of the Cu_2Se thin films from the reported data.

Acknowledgements

P. Fan, X. L. Huang and T. B. Chen contributed equally. This work is supported by National Natural Science Foundation of China (11604212), Guangdong Basic and Applied Basic Research Foundation (2020A1515010515), and Shenzhen Key Lab Fund (ZDSYS 20170228105421966). The authors are also thankful for the assistance on HAADF-STEM observation received from the Electron Microscope Center of the Shenzhen University.

References

[1] P. F. Qiu, X. Shi, L. D. Chen, Cu-based thermoelectric materials, Energy Storage Mater., 2016, 3, 8.

[2] G. M. Chen, W. Xu, D. B. Zhu, Recent advances in organic polymer thermoelectric composites, J. Mater. Chem. C, 2017, 5, 4350.

[3] N. Toshima, Recent progress of organic and hybrid thermoelectric materials, Synth. Met., 2017, 225, 3.

[4] Y. Deng, H. Liang, Y. Wang, Z. Zhang, M. Tan, J. Cui, Growth and transport properties of oriented bismuth telluride films, J. Alloys Compd., 2011, 509, 5683.

[5] X. Mu, H. Zhou, D. He, W. Zhao, P. Wei, W. Zhu, X. Nie, H. Liu, Q. Zhang, Enhanced electrical properties of stoichiometric $Bi_{0.5}Sb_{1.5}Te_3$ film with high-crystallinity via layer-by-layer in-situ growth, Nano Energy, 2017, 33, 55.

[6] T. Park, C. Park, B. Kim, H. Shin, E. Kim, Flexible PEDOT electrodes with large thermoelectric power factors to generate electricity by the touch of fingertips, Energ. Environ. Sci., 2013, 6, 788.

[7] T. Horide, Y. Murakami, Y. Hirayama, M. Ishimaru, K. Matsumoto, Thermoelectric Property in Orthorhombic-Domained SnSe Film, ACS Appl. Mater. Interfaces, 2019, 11, 27057.

[8] S. Lal, K. M. Razeeb, D. Gautam, Enhanced Thermoelectric Properties of Electrodeposited Cu-Doped Te Films, ACS Appl. Energy Mater., 2020, 3, 3262.

[9] S. J. Kim, J. H. We, B. J. Cho, A wearable thermoelectric generator fabricated on a glass fabric, Energ. Environ. Sci., 2014, 7, 1959.

[10] I. Chowdhury, R. Prasher, K. Lofgreen, G. Chrysler, S. Narasimhan, R. Mahajan, D. Koester, R. Alley, R. Venkatasubramanian, On-chip cooling by superlattice-based thin-film thermoelectrics, Nat. Nanotechnol., 2009, 4, 235.

[11] S. N. Jin, T. T. Sun, Y. C. Fan, L. J. Wang, M. F. Zhu, J. P. Yang, W. Jiang, Synthesis of freestanding PEDOT:PSS/PVA Ag NPs nanofiber film for high-performance flexible thermoelectric generator, Polymer, 2019, 167, 102.

[12] R. Venkatasubramanian, E. Siivola, T. Colpitts, B. O'Quinn, Thin-film thermoelectric devices with high room-temperature figures of merit, Nature, 2001, 413, 597.

[13] B. Y. Yoo, C. K. Huang, J. R. Lim, J. Herman, M. A. Ryan, J. P. Fleurial, N. V. Myung, Electrochemically deposited thermoelectric n-type Bi_2Te_3 thin films, Electrochim. Acta, 2005, 50, 4371.

[14] S. Yonezawa, T. Tabuchi, M. Takashiri, Atomic composition changes in bismuth telluride thin films by thermal annealing and estimation of their thermoelectric properties using experimental analyses and first-principles calculations, J. Alloys Compd., 2020, 841, 155697.

[15] Z. H. Wu, E. Mu, Z. X. Che, Y. Liu, F. Y. Sun, X. W.Wang, Z. Y. Hu, Nanoporous (00l)-oriented Bi_2Te_3 nanoplate film for improved thermoelectric performance, J. Alloys Compd., 2020, 828, 154239.

[16] S. D. Kang, J. H. Pohls, U. Aydemir, P. F. Qiu, C. C. Stoumpos, R. Hanus, M. A. White, X. Shi, L. D. Chen, M. G. Kanatzidis, G. J. Snyder, Enhanced stability and thermoelectric figure-of-merit in copper selenide by lithium doping, Mater. Today Phys., 2017, 1, 7.

[17] L. D. Zhao, S. H. Lo, Y. S. Zhang, H. Sun, G. J. Tan, C. Uher, C. Wolverton, V. P. Dravid, M. G. Kanatzidis, Ultralow thermal conductivity and high thermoelectric figure of merit in SnSe crystals, Nature, 2014, 508, 373.

[18] L. D. Zhao, G. J. Tan, S. Q Hao, J. Q. He, Y. L. Pei, H. Chi, H. Wang, S. K. Gong, H. B. Xu, V.P. Dravid, C. Uher, G. J. Snyder, C. Wolverton, M. G. Kanatzidis, Ultrahigh power factor and thermoelectric performance in hole-doped single-crystal SnSe, Science, 2016, 351, 141.

[19] Asfandiyar, B. W. Cai, L. D. Zhao, J. F. Li, High thermoelectric figure of merit ZT > 1 in SnS polycrystals, J. Materiomics, 2020, 6, 77.

[20] F. H. Shen, Y. Y. Zheng, L. Miao, C. Y. Liu, J. Gao, X. Y. Wang, P. F. Liu, K. Yoshida, H. F. Cai, Boosting High Thermoelectric Performance of Ni-Doped $Cu_{1.9}S$ by Significantly Reducing Thermal Conductivity, ACS Appl. Mater. Interfaces, 2020, 12, 8385.

[21] C. Chang, M. H. Wu, D. S. He, Y. L. Pei, C. F. Wu, X. F. Wu, H. L. Yu, F. Y. Zhu, K. D. Wang, Y. Chen, L. Huang, J. F. Li, J. Q. He, L. D. Zhao, 3D charge and 2D phonon transports leading to high out-of-plane ZT in n-type SnSe crystals, Science, 2018, 360, 778.

[22] B. Gahtori, S. Bathula, K. Tyagi, M. Jayasimhadri, A. K. Srivastava, S. Singh, R. C. Budhani, A. Dhar, Giant enhancement in thermoelectric performance of copper selenide by incorporation of different nanoscale dimensional defect features, Nano Energy, 2015, 13, 36.

[23] D. W. Yang, X. L. Su, F. C. Meng, S. Wang, Y. G. Yan, J. H. Yang, J. He, Q. J. Zhang, C. Uher, M. G. Kanatzidis, X. F. Tang, Facile room temperature solventless synthesis of high thermoelectric performance Ag_2Se via a dissociative adsorption reaction, J. Mater. Chem. A, 2017, 5, 23243.

[24] H. L. Liu, X. Shi, F. F. Xu, L. L. Zhang, W. Q. Zhang, L. D. Chen, Q. Li, C. Uher, T. Day , G. J. Snyder, Copper ion liquid-like thermoelectrics, Nat. Mater., 2012, 11, 422.

[25] H. L. Liu, X. Yuan, P. Lu, X. Shi, F. F. Xu, Y. He, Y. Tang, S. Q. Bai, W. Q. Zhang, L. D. Chen, Y. Lin , L. Shi , H. Lin, X. Y. Gao, X. M. Zhang, H. Chi, C. Uher, Ultrahigh thermoelectric performance by electron and phonon critical scattering in $Cu_2Se_{1-x}I$, Adv. Mater., 2013, 25, 6607.

[26] H. L. Liu, X. Shi, M. Kirkham, H. Wang, Q. Li, C. Uher, W. Q. Zhang, L. D. Chen, Structure-transformation-induced abnormal thermoelectric properties in semiconductor copper selenide, Mater. Lett., 2013, 93, 121.

[27] T. W. Day, K. S. Weldert, W. G. Zeier, B. R. Chen, S. L. Moffitt, U. Weis, K. P. Jochum, M. Panthöfer, M. J. Bedzyk, G. J. Snyder, W. Tremel, Influence of compensating defect formation on the doping efficiency and thermoelectric properties of $Cu_{2-y}Se_{1-x}Br_x$, Chem. Mater., 2015, 27, 7018.

[28] W. W. Liao, L. Yang, J. Chen, D. L. Zhou, X. L. Qu, K. Zheng, G. Han, J. B. Zhou, M. Hong, Z. G. Chen, Realizing Bi-doped α-Cu_2Se as a promising near-room-temperature thermoelectric material, Chem. Eng. J., 2019, 371, 593.

[29] Y. Lu, Y. F. Ding, Y. Qiu, K. F. Cai, Q. Yao, H. J. Song, L. Tong, J. Q. He, L. D. Chen, Good performance and flexible PEDOT:PSS/Cu_2Se nanowire thermoelectric composite films, ACS Appl. Mater. Interfaces, 2019, 11, 12819.

[30] J. D. Forster, J. J. Lynch, N. E. Coates, J. Liu, H. Jang, E. Zaia, M. P. Gordon, M. Szybowski, A. Sahu, D. G. Cahill, J. J. Urban, Solution-Processed Cu_2Se Nanocrystal Films with Bulk-Like Thermoelectric Performance, Sci. Rep., 2017, 7, 2765.

[31] Z. P.Wu, J. L. Wu, Y. Li, G. J. Li, Effect of Cu content on electrical properties of evaporated Cu-Se thermoelectric films, Ceram. Int., 2020, 46, 21617.

[32] J. A. Perez-Taborda, L. Vera, O. Caballero-Calero, E. O. Lopez, J. J. Romero, D. G. Stroppa, F. Briones, M. Martin-Gonzalez, Pulsed hybrid reactive magnetron sputtering for high ZT Cu_2Se thermoelectric films, Adv. Mater. Technol., 2017, 2, 1700012.

[33] Z. Y. Lin, C. Hollar, J. S. Kang, A. Yin, Y. L. Wang, H. Y. Shiu, Y. Huang, Y. J. Hu, Y. L. Zhang, X. F. Duan, A solution processable high-performance thermoelectric copper selenide thin film, Adv. Mater., 2017, 29, 1606662.

[34] M. R. Scimeca, F. Yang, E. Zaia, N. Chen, P. Zhao, M. P. Gordon, J. D. Forster, Y. S. Liu, J. H. Guo, J. J. Urban, A. Sahu, Rapid stoichiometry control in Cu_2Se thin films for room-temperature power factor improvement, ACS Appl. Energy Mater., 2019, 2, 1517.

[35] L. Song, J. W. Zhang, B. B. Iversen, Enhanced thermoelectric properties of SnSe thin films grown by single-target magnetron sputtering, J. Mater. Chem. A, 2019, 7, 17981.

[36] R. Lan, S. L. Otoo, P. Yuan, P. F. Wang, Y. Y. Yuan, X. B. Jiang, Thermoelectric properties of Sn doped GeTe thin films, Appl. Sur. Sci., 2020, 507, 145025.

[37] L. Francioso, C. D. Pascalia, I. Farella, C. Martucci, P. Cretì, P. Siciliano, A. Perrone, Flexible thermoelectric generator for ambient assisted living wearable biometric sensors, J. Power Sources, 2011, 196, 3239.

[38] Y. Sun, M. Christensen, S. Johnsen, N. V. Nong, Y. Ma, M. Sillassen, E. Zhang, A. E. C. Palmqvist, J. Bøttiger, B. B. Iversen, Low-cost high-performance zinc antimonide thin films for thermoelectric applications, Adv. Mater., 2012, 24, 1693.

[39] J. L. Yu, B. Liu, T. Zhang, Z. T. Song, S. L. Feng, B. Chen, Effects of Ge doping on the properties of Sb_2Te_3 phase-change thin films, Appl. Sur. Sci., 2007, 253, 6125.

[40] Q. Wang, Y. Liang, H. Yao, J. W. Li, B. Wang, J. Wang, Emerging negative differential resistance effect and novel tunable electronic behaviors of the broken-gap $KAgSe/SiC_2$ van der Waals heterojunction, J. Mater. Chem. C, 2020, 8, 8107.

[41] Q. Wang, J. W. Li, Y. H. Nie, F. M. Xu, Y. J. Yu, B. Wang, Pure spin current and phonon thermoelectric transport in a triangulene-based molecular junction, Phys. Chem. Chem. Phys., 2018, 20, 15736.

[42] W. T. Wang, Z. H. Zheng, F. Li, C. Li, P. Fan, J. T. Luo, B. Li, Synthesis process and thermoelectric properties of n-type tin selenide thin films, J. Alloys Compd., 2018, 763, 960.

[43] E. R. Sittner, K. S. Siegert, P. Jost, C. Schlockermann, F. R. L. Lange, M. Wuttig, $(GeTe)_x$-$(Sb_2Te_3)_{1-x}$ phase-change thin films as potential thermoelectric materials, Phys. Status Solidi A, 2013, 210, 147.

[44] Y. Z. Li, F. Li, G. X. Liang, W. L. Zheng, Y. M. Xu, Z. H. Zheng, P. Fan, Sb_2Se_3 thin films fabricated by thermal evaporation deposition using the powder prepared via mechanical alloying, Sur. Coat. Technol., 2019, 358, 1013.

[45] S. D. Kang, S. A. Danilkin, U. Aydemir, M. Avdeev, A. Studer, G. J. Snyder, Apparent critical phenomena in the superionic phase transition of $Cu_{2-x}Se$, New J. Phys., 2016, 18, 013024.

[46] P. Fan, P. C. Zhang, G. X. Liang, F. Li, Y. X. Chen, J. T. Luo, X. H. Zhang, S. Chen, Z. H. Zheng, High-performance bismuth telluride thermoelectric thin films fabricated by using the two-step single-source thermal evaporation, J. Alloys Compd., 2020, 819, 153027.

[47] F. K. Lotgering, Topotactical reactions with ferrimagnetic oxides having hexagonal crystal structures-I, J. Inorg. Nucl. Chem., 1959, 9, 113.

[48] J. K. Chen, H. Y. Hu, F. Q. Meng, T. Yajima, L. X. Yang, B. H. Ge, X. Y. Ke, J. O. Wang, Y. Jiang, N. F. Chen, Overlooked transportation anisotropies in *d*-band correlated rare-earth perovskite nickelates, Matter, 2020, 2, 1296.

[49] J. K. Chen, H. Y. Hu, J. O. Wang, T. Yajima, B. H. Ge, X. Y. Ke, H. L. Dong, Y. Jiang, N. F. Chen, Overcoming synthetic metastabilities and revealing metal-to-insulator

transition & thermistor bi-functionalities for *d*-band correlation perovskite nickelates, Mater. Horiz., 2019, 6, 788.

[50] J. K. Chen, H. Y. Hu, J. O. Wang, C. Liu, X. L. Liu, Z. Li, N. F. Chen, A *d*-band electron correlated thermoelectric thermistor established in metastable perovskite family of rare-earth nickelates, ACS Appl. Mater. Interfaces 2019, 11, 34128.

[51] H. J. Shang, F. Z. Ding, G. C. Li, L. Wang, F. Qu, H. L. Zhang, Z. B. Dong, H. Zhang, Z. S. Gao, W. W. Zhou, H. W. Gu, High performance co-sputtered Bi_2Te_3 thin films with preferred orientation induced by MgO substrates, J. Alloys Compd., 2017, 726, 532.

[52] W. H. Shi, J. S. Lian, Facile synthesis of copper selenide with fluffy intersected-nanosheets decorating nanotubes structure for efficient oxygen evolution reaction, Inter. J. Hydrogen Energ., 2019, 44, 22983.

[53] L. J. Zhu, H. J. Xie, Y. X, Liu, D. Y. Chen, M. Y. Bian, W. J. Zheng, Novel ultralong hollow hyperbranched $Cu_{2-x}Se$ with nanosheets hierarchical structure: Preparation, formation mechanism and properties, J. Alloys Compd., 2019, 802, 430.

[54] W. D. Liu, L. Yang, Z. G. Chen, J. Zou, Promising and eco-friendly Cu_2X-based thermoelectric materials: progress and applications, Adv. Mater., 2020, 32, 1905703.

[55] F. Jia, S. Zhang, X. K. Zhang, X. L. Peng, H. T. Zhang, Y. Xiang, Sb-Triggered β-to-α Transition: Solvothermal Synthesis of Metastable α-Cu_2Se, Chem. Eur. J., 2014, 20, 15941.

[56] Y. D. Li, P. Fan, Z. H. Zheng, J. T. Luo, G. X. Liang, S. Z. Guo, The influence of heat treatments on the thermoelectric properties of copper selenide thin films prepared by ion beam sputtering deposition, J. Alloys Compd., 2016, 658, 880.

[57] K. S. Urmila, T. N. Asokan, R. R. Philip, V. Ganesan, G. S. Okram, B. Pradeep, Structural, optical, electrical and low temperature thermoelectric properties of degenerate polycrystalline Cu_7Se_4 thin films, Phys. Status Solidi B, 2014, 251, 689.

[58] Y. H. Lv, J. K. Chen, R. K. Zheng, X. Shi, J. Q. Song, T. S. Zhang, X. M. Li, L. D. Chen, (001)-oriented $Cu_{2-y}Se$ thin films with tunable thermoelectric performances grown by pulsed laser deposition, Ceram. Int., 2015, 41, 7439.

[59] A. Ghosh, C. Kulsi, D. Banerjee, A. Mondal, A. Ghosh, C. Kulsi, D. Banerjee, A. Mondal, Galvanic synthesis of $Cu_{2-x}Se$ thin films and their photocatalytic and thermoelectric properties, Appl. Sur. Sci., 2016, 369, 525.

[60] M. Q. Yang, z. W. Shen, X. Q. Liu, W. Wang, Electrodeposition and thermoelectric properties of Cu-Se binary compound films, J. Electron. Mater., 2016, 45, 1974.